



Measurement of interferences associated with the detection of the hydroperoxy radical in the atmosphere using laser-induced fluorescence

Michelle M. Lew¹, Sebastien Dusanter^{2,3}, and Philip S. Stevens^{1,3}

(1) Department of Chemistry, Indiana University, Bloomington, IN, USA

(2) IMT Lille Douai, Univ. Lille, SAGE - Département Sciences de l'Atmosphère et Génie de l'Environnement, 59000 Lille, France

(3) School of Public and Environmental Affairs, Indiana University, Bloomington, IN, USA

Correspondence to: Philip S. Stevens (pstevens@indiana.edu)

1 **Abstract.** One technique used to measure concentrations of the hydroperoxy radical (HO_2) in the atmosphere
2 involves chemically converting it to OH by addition of NO and subsequent detection of OH. However, some
3 organic peroxy radicals (RO_2) can also be rapidly converted to HO_2 (and subsequently OH) in the presence of
4 NO, interfering with measurements of ambient HO_2 radical concentrations. This interference must be
5 characterized for each instrument to determine to what extent various RO_2 radicals interfere with measurements
6 of HO_2 and to assess the impact of this interference on past measurements. The efficiency of RO_2 to HO_2
7 conversion for the Indiana University Laser-Induced Fluorescence – Fluorescence Assay by Gas Expansion (IU-
8 FAGE) instrument was measured for a variety of RO_2 radicals. Known quantities of OH and HO_2 radicals were
9 produced from the photolysis of water vapor at 184.9 nm, and RO_2 radicals were produced by the reaction of
10 several volatile organic compounds with OH. The conversion efficiency of RO_2 radicals to HO_2 was measured
11 when NO was added to the sampling cell for conditions employed during several previous field campaigns. For
12 these conditions, approximately 80% of alkene derived RO_2 radicals and 20% of alkane derived RO_2 radicals were
13 converted to HO_2 . Based on these measurements, interferences from various RO_2 radicals contributed to
14 approximately 35% of the measured HO_2 signal during the Mexico City Metropolitan Area (MCMA) 2006
15 campaign, where the measured VOCs consisted of a mixture of saturated and unsaturated species. However, this
16 interference can contribute more significantly to the measured HO_2 signal in forested environments dominated by
17 unsaturated biogenic emissions such as isoprene.



1 **1 Introduction**

2 The hydroxyl radical (OH) is one of the primary oxidants in the atmosphere (Levy, 1972). The reaction of OH
3 radicals with volatile organic compounds (VOCs) leads to the production of peroxy radicals, both the hydroperoxy
4 radical (HO₂) and organic peroxy radicals (RO₂), which in the presence of nitrogen oxides (NO_x = NO + NO₂)
5 can lead to the production of ozone and secondary organic aerosols in the atmosphere. As a consequence, the
6 development of effective control strategies for the formation of these pollutants requires an accurate understanding
7 of the OH, HO₂, and RO₂ radical chemistry in the atmosphere. Measurements of OH and HO₂ (together HO_x) can
8 provide a robust test of our understanding of this complex oxidation chemistry.

9 Multiple field campaigns have been conducted over the years measuring OH and HO₂ radicals in both
10 urban and forested environments. While much attention has been focused on discrepancies between measured and
11 modeled OH concentrations (Rohrer et al., 2014), the agreement between measured and modeled HO₂
12 concentrations has been highly variable. In urban environments, measured HO₂ concentrations were sometimes
13 found to agree with model predictions (Shirley et al., 2006; Emmerson et al., 2007; Dusanter et al., 2009b;
14 Michoud et al., 2012; Lu et al., 2013; Ren et al., 2013; Griffith et al., 2016), while other times the measurements
15 were found to be both lower (George et al., 1999; Konrad et al., 2003) and higher than model predictions (Martinez
16 et al., 2003; Ren et al., 2003; Emmerson et al., 2005; Kanaya et al., 2007a; Chen et al., 2010; Sheehy et al., 2010;
17 Czader et al., 2013; Griffith et al., 2016). In forested environments, measured HO₂ concentrations were sometimes
18 found to agree with model predictions (Tan et al., 2001; Ren et al., 2005; 2006), but were often found to be either
19 lower (Carslaw et al., 2001; Kanaya et al., 2007b; Whalley et al., 2011; Kanaya et al., 2012; Mao et al., 2012;
20 Griffith et al., 2013), or higher than model predictions (Carslaw et al., 2001; Kubistin et al., 2010; Kim et al.,
21 2013; Hens et al., 2014).

22 These results question our understanding of HO_x radical chemistry and the ability of models to simulate
23 future changes in the chemical composition of the atmosphere. However, a recent intercomparison of several
24 instruments measuring HO₂ found that the agreement between the different instruments was variable, although
25 the measurements were highly correlated (Fuchs et al., 2010). While the differences were within the combined
26 uncertainties of the measurements, there were several measurement periods when the differences could not be
27 explained by instrumental uncertainties. These results suggested the possibility of potential interferences in the
28 HO₂ measurement technique.

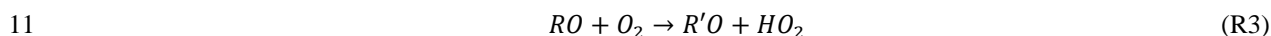
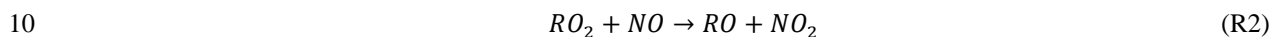
29 Laser-induced fluorescence using the Fluorescence Assay by Gas Expansion technique (LIF-FAGE) is a
30 common method for measuring HO₂ radicals in the atmosphere. In this technique HO₂ radicals are measured



1 indirectly after sampling ambient air at low pressure through chemical conversion to OH by addition of NO as
2 shown in reaction R1 and subsequent detection of OH by LIF:



4 It was previously believed that the detection of HO₂ radicals using the LIF-FAGE technique was free from
5 interferences from the reaction of RO₂ radicals with NO, as model simulations and measurements suggested that
6 the rate of conversion of RO₂ radicals to HO₂ by reactions R2 and R3 and subsequent conversion to OH through
7 reaction R1 was negligible due to the slow rate of reaction R3 under the reduced oxygen concentration in the low
8 pressure LIF-FAGE cell and the short reaction time between injection of NO and detection of OH (Heard and
9 Pilling, 2003).



12 For example, RO₂ radicals produced from the OH-initiated oxidation of small alkanes were found to produce a
13 negligible yield of HO₂ (Stevens et al., 1994; Kanaya et al., 2001; Tan et al., 2001; Creasey et al., 2002; Holland
14 et al., 2003).

15 However, recent laboratory studies have shown that there are interferences associated with measurements
16 of HO₂ using this technique from the conversion of RO₂ radicals derived from the OH-initiated oxidation of
17 alkenes and aromatics to HO₂ (and subsequently OH) by reaction with NO. Measured RO₂ to HO₂ conversion
18 efficiencies of 95% for the peroxy radicals derived from the OH-initiated oxidation of propene and 86% for the
19 peroxy radicals derived from the OH-initiated oxidation of benzene have been reported (Fuchs et al., 2011). The
20 high conversion efficiency of alkene-based peroxy radicals to HO₂ is due to the ability of the β-hydroxyalkoxy
21 radicals produced from reaction R2 to rapidly decompose forming a hydroxyalkyl radical which then reacts rapidly
22 with O₂ leading to the production of a carbonyl compound and HO₂ (Fuchs et al., 2011; Whalley et al., 2013). The
23 conversion efficiency depends on the instrumental characteristics and the configurations employed (Fuchs et al.,
24 2011; Whalley et al., 2013). As a result, this interference must be characterized for all LIF-FAGE instruments for
25 the accurate analysis of ambient HO₂.

26 This paper will describe the characterization of the RO₂ interferences associated with the Indiana
27 University LIF-FAGE instrument under several past campaign configurations. These include the Mexico City
28 Metropolitan Area (MCMA) campaign in 2006 (Dusanter et al., 2009a; 2009b), the Community Atmosphere-
29 Biosphere Interactions EXperiment (CABINEX) in 2009 (Griffith et al., 2013), and the California Research at
30 the Nexus of Air Quality and Climate Change campaign in Los Angeles (CalNex-LA) in 2010 (Griffith et al.,



1 2016). The impact of this interference on the previously published results from the MCMA-2006 campaign and a
2 reanalysis of these HO₂ measurements will be discussed.

3 2 Experimental Section

4 2.1 Instrument description

5 The Indiana University LIF-FAGE instrument (IU-FAGE) has been described in detail previously (Dusanter et
6 al., 2008; 2009a; Griffith et al., 2013; 2016). In the LIF-FAGE technique, OH radicals are detected by laser-
7 induced fluorescence after expansion of ambient air to low pressure. This enhances the OH fluorescence lifetime,
8 allowing temporal filtering of the fluorescence from laser scatter (Heard and Pilling, 2003). A diagram of the IU-
9 FAGE detection cell is illustrated in Fig. 1. Ambient air is expanded through an orifice between 0.635 mm and
10 1.016 mm diameter located at the top of a cylindrical nozzle (5 cm in diameter and 20 cm long). The size of the
11 orifice was kept unchanged during each campaign but was varied between the different campaigns reported here.
12 Two scroll pumps (Edwards XDS 35i) connected in parallel maintain a pressure inside the cell between 4 and 7.5
13 Torr depending on the sampling size of the orifice and the pumping speed, resulting in a flow rate between 3 and
14 10 SLPM through the sampling nozzle.

15 The original IU-FAGE laser system used in this study consisted of a Spectra Physics Navigator II
16 YHP40-532Q diode-pumped Nd:YAG laser that produced approximately 5.5W of radiation at 532 nm at a
17 repetition rate of 5 kHz. This laser pumped a Lambda Physik Scanmate 1 dye laser (Rhodamine 640, 0.25 g L⁻¹
18 in isopropanol) that produced tunable radiation around 616 nm, which was frequency doubled to generate 2 to 20
19 mW of radiation at 308 nm (~20 ns pulse width). This laser system was recently replaced with a Spectra Physics
20 Navigator II YHP40-532Q that produces approximately 8 W of radiation at 532 nm at a repetition rate of 10 kHz
21 that pumps a Sirah Credo Dye laser (255 mg/L of Rhodamine 610 and 80 mg/L of Rhodamine 101 in ethanol),
22 resulting in 40 to 100 mW of radiation at 308 nm. After exiting the dye laser, the beam was focused onto the
23 entrance of a 12 m optical fiber to transmit the radiation to the sampling cell. In the detection cell, the laser crosses
24 the expanded air perpendicular to the flow in a White cell configuration with approximately 24 passes.

25 OH radicals are excited using the $A^2\Sigma^+ \nu'=0 \leftarrow X^2\Pi \nu''=0$ transition near 308 nm (Stevens et al., 1994).
26 The net signal is measured by turning the wavelength on- and off-resonance in successive modulation cycles. A
27 reference cell where OH is produced by thermal dissociation of water vapor is used to ensure that the laser is tuned
28 on and off the OH transition. The OH fluorescence is detected using a microchannel plate photomultiplier tube
29 (MCP-PMT) detector (Hamamatsu R5946U-50), a preamplifier (Stanford Research System SR445) and a gated

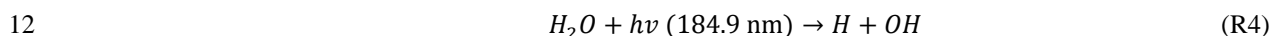


1 photon counter (Stanford Research Systems SR 400). The MCP-PMT is switched off during the laser pulse
2 through the use of electronic gating allowing the OH fluorescence to be temporally filtered from laser scattered
3 light.

4 A Teflon injector located approximately 2.5 cm below the inlet and 17.5 cm above the detection axis
5 (Fig. 1) allowed for the addition of NO (Matheson, 99.8%) to convert ambient HO₂ to OH through reaction R1.
6 The fraction of HO₂ (C_{HO2}) converted into OH was measured during calibration experiments (Dusanter et al.,
7 2008). The NO flow (approximately 1-3×10¹³ cm⁻³) maximized the conversion of HO₂ into OH while minimizing
8 the removal of OH by the OH + NO reaction.

9 2.2 Instrument Calibration for OH and HO₂

10 The IU-FAGE instrument is calibrated by producing known quantities of OH and HO₂ radicals from the photolysis
11 of water vapor in air (reactions R4 and R5) (Dusanter et al., 2008):

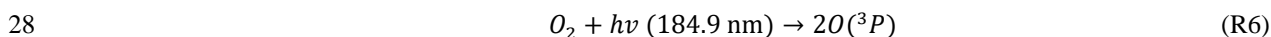


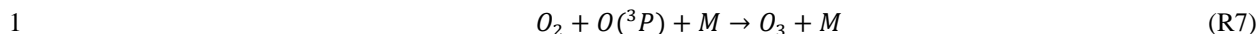
14 The calibration source consists of an aluminum flow reactor (1.27×1.27×30 cm) equipped with quartz windows
15 on two sides (Fig. 2). The light source consists of a low-pressure mercury lamp (UVP Inc.) housed in an aluminum
16 cartridge that is continuously purged with dry nitrogen to prevent light absorption by gases in addition to helping
17 to stabilize the lamp temperature. The radiation from the lamp passes through a bandpass filter centered at 185
18 nm (Acton Research) prior to entering the reactor and is detected by a photodiode. The lamp housing can be
19 adjusted along the length of the calibrator to measure the loss of radicals between the source region and the exit
20 of the calibrator.

21 The concentration of OH and HO₂ radicals produced by the calibration source can be determined from
22 the following equation:

$$23 \quad [OH] = [HO_2] = [H_2O] \cdot \sigma_{H_2O} \cdot \varphi_{OH+H} \cdot F \cdot t \quad (1)$$

24 In this equation φ_{OH+H} is the quantum yield of OH from water photolysis, and σ_{H_2O} is the absorption cross section
25 of water (7.14×10^{-20} cm² molecule⁻¹ (Cantrell et al., 1997; Hofzumahaus et al., 1997; Creasey et al., 2000)). The
26 product of the photon flux (F) and the photolysis time (t) can be determined from oxygen actinometry, as the
27 photolysis of oxygen at 185 nm leads to the production of ozone (reactions R6 and R7) (Okabe, 1978):





2 The concentration of HO_x radicals can thus be calculated from measured concentrations of water and ozone using
3 Eq. (2) (Heard and Pilling, 2003; Holland et al., 2003):

4
$$[OH] = [HO_2] = [H_2O] \cdot \sigma_{H_2O} \cdot \varphi_{OH+H} \cdot \frac{[O_3]}{\varphi_{O_3} \cdot \sigma_{O_2} \cdot [O_2]} \quad (2)$$

5 Here φ_{O_3} is the quantum yield of O₃ from oxygen photolysis and σ_{O_2} is the absorption cross sections of O₂,
6 which must be experimentally determined for each penlamp due to the overlap of the highly structured absorption
7 spectrum of O₂ and the lineshape of the emission at 184.9 nm. The lineshape depends on the operating conditions
8 of the lamp as a result of line reversal and potential fluorescence of the fused silica envelope (Cantrell et al., 1997;
9 Hofzumahaus et al., 1997; Lanzendorf et al., 1997).

10 2.3 Measurement of the RO₂ conversion efficiency to HO₂

11 Various alkenes (isoprene, methyl vinyl ketone, methacrolein, methyl ethyl ketone, ethene, trans-2-butene,
12 tetramethylethylene), alkanes (propane, butane, octane), and aromatic compounds (toluene) were used to measure
13 the conversion efficiency of RO₂ radicals to HO₂. These VOCs were added to the main calibrator flow
14 approximately 190 ms prior to the radical source to ensure that the added VOC was well mixed into the humid air
15 flow before photolysis within the calibration source. The concentration of each VOC added to the calibrator was
16 increased to react and remove the majority of the OH produced in the calibrator, resulting in RO₂ concentrations
17 that were approximately equal to the concentration of OH reacted away. These RO₂ radicals are then sampled into
18 the IU-FAGE instrument. Addition of NO inside the detection axis converts a fraction of the RO₂ radicals to HO₂
19 through reactions R2 and R3. Since RO₂ is produced together with HO₂ in the calibrator, there is a subsequent
20 conversion of both RO₂ and HO₂ into OH in the IU-FAGE cell, which is then detected by LIF.

21 Figure 3 illustrates two typical experiments designed to measure the conversion efficiency of RO₂
22 radicals to HO₂ in the IU-FAGE instrument. The total HO_x signal is defined as the sum of the total OH (S_{OH}) and
23 HO₂ (S_{HO₂}) produced by the mercury penlamp in the absence of the added VOC (Eq. (3)):

24
$$S_{HO_x} = S_{HO_2} + S_{OH} \quad (3)$$

25 The OH concentration produced by the penlamp is measured at the beginning, middle, and at the end of each
26 experiment to ensure that the concentrations remained stable (experimental mode 1 in Fig. 3). Once the OH signal



1 (S_{OH}) stabilizes, NO is added internally to the detection cell to convert HO_2 into OH and measure the total HO_x
 2 signal (S_{HO_x}) (mode 2 in Fig. 3). The conversion efficiency of HO_2 to OH is defined by Eq. (4):

$$3 \quad C_{HO_2 \rightarrow OH} = \frac{S_{HO_x} - S_{OH}}{S_{OH_0}} = \frac{S_{HO_2}}{S_{OH_0}} \quad (4)$$

4 S_{OH_0} is the OH signal after accounting for the loss of OH on the walls of the calibrator (approximately 20%). The
 5 wall loss for HO_2 is negligible in the calibrator (Dusanter et al., 2008).

6 Next, internal NO addition is stopped and the OH signal is measured again to ensure the stability of
 7 radical production during the experiment. The VOC is then added to the calibration system resulting in a decrease
 8 in the observed OH signal (mode 3 in Fig. 3). The remaining OH signal in the presence of the VOC is denoted as
 9 S_{OH+VOC} . For alkenes such as isoprene, the fast reaction with OH results in an almost total removal of OH radicals
 10 from the calibration source and S_{OH+VOC} is close to zero. However, for less reactive alkanes such as butane, the
 11 added VOC concentration was often not sufficient to completely remove OH radicals due to the short reaction
 12 time in the calibrator, resulting in a non-zero S_{OH+VOC} signal. The conversion efficiency in which OH radicals are
 13 converted to RO_2 radicals (C_{OH+VOC}) is defined by Eq. (5), derived from integrating the expressions for the rate of
 14 OH loss and the rate of RO_2 production from the OH +VOC reaction:

$$15 \quad C_{OH+VOC} = \frac{[RO_2]}{[OH]_0} = \frac{F_{OH} - k_w t}{F_{OH}} (1 - e^{-F_{OH}}) \quad F_{OH} = \ln\left(\frac{S_{OH_0}}{S_{OH+VOC}}\right) \quad (5)$$

16 Here $k_w t$ is the product of the rate constant for reaction of OH radicals on the wall of the calibration source with
 17 the reaction time t , reflecting the measured loss of OH on the walls of the calibrator (Dusanter et al., 2008).

18 The subsequent addition of NO to the detection cell will convert a fraction of RO_2 radicals and HO_2
 19 radicals to OH (mode 4 in Fig. 3). The conversion efficiency of RO_2 to OH ($C_{RO_2 \rightarrow OH}$) is determined by
 20 multiplying the fraction of RO_2 radicals converted to HO_2 ($f_{RO_2 \rightarrow HO_2}$) with the conversion efficiency of HO_2 to
 21 OH ($C_{HO_2 \rightarrow OH}$):

$$22 \quad C_{RO_2 \rightarrow OH} = f_{RO_2 \rightarrow HO_2} \cdot C_{HO_2 \rightarrow OH} \quad (6)$$

23 The signal due to RO_2 radicals (S_{RO_2}) is defined as the original OH signal (S_{OH_0}) multiplied by the conversion
 24 efficiency of OH radicals to RO_2 radicals (C_{OH+VOC}) and multiplied by the conversion efficiency of RO_2 to OH
 25 ($C_{RO_2 \rightarrow OH}$) (Eq. (7)):

$$26 \quad S_{RO_2} = S_{OH_0} \cdot C_{OH+VOC} \cdot C_{RO_2 \rightarrow OH} \quad (7)$$



1 For OH +VOC reactions that lead to the production of HO₂ with a yield of y (OH + benzene and toluene for
 2 example (Klotz et al., 1998; Nehr et al., 2011)), the OH to RO₂ conversion efficiency (C_{OH+VOC}) must be multiplied
 3 by the overall yield ($1-y$) of RO₂ radicals produced from the OH +VOC reaction. Taking this yield into account,
 4 the signals due to RO₂ and HO₂ radicals become:

$$5 \quad S_{RO_2} = S_{OH_0} \cdot C_{OH+VOC} \cdot (1-y) \cdot C_{RO_2 \rightarrow OH} \quad (7a)$$

$$6 \quad S_{HO_2 \text{ total}} = S_{OH_0} \cdot C_{OH+VOC} \cdot y \cdot C_{HO_2 \rightarrow OH} + S_{HO_2} \quad (8)$$

7 The measured OH signal under these conditions (S_{RO_x}) reflects the contribution of RO₂, HO₂, and unreacted OH
 8 radicals (experimental mode 4):

$$9 \quad S_{RO_x} = S_{RO_2} + S_{HO_2 \text{ total}} + S_{OH+VOC} \quad (9)$$

$$10 \quad S_{RO_x} = (S_{OH_0} \cdot C_{OH+VOC} \cdot (1-y) \cdot C_{RO_2 \rightarrow OH}) + (S_{OH_0} \cdot C_{OH+VOC} \cdot y \cdot C_{HO_2 \rightarrow OH} + S_{HO_2}) + S_{OH+VOC} \quad (9a)$$

11 Combining equations 3, 6, and 9a results in an expression for the fraction of RO₂ radicals converted to HO₂
 12 ($f_{RO_2 \rightarrow HO_2}$) that can be expressed as the measured signals for each experimental mode (S_{OH} , S_{HO_x} , S_{OH+VOC} ,
 13 S_{RO_x}) as seen in Eq. (10):

$$14 \quad f_{RO_2 \rightarrow HO_2} = \frac{S_{RO_x} - S_{HO_x} + S_{OH} - S_{OH+VOC} - S_{OH_0} \cdot C_{OH+VOC} \cdot y \cdot C_{HO_2 \rightarrow OH}}{S_{OH_0} \cdot C_{OH+VOC} \cdot (1-y) \cdot C_{HO_2 \rightarrow OH}} \quad (10)$$

15 When the yield of HO₂ from the OH + VOC reaction is zero ($y = 0$), and under conditions where all the OH
 16 radicals are converted to RO₂ ($S_{OH+VOC} = 0$), the above equation (with Eq. 3 and 4) simplifies to the following:

$$17 \quad f_{RO_2 \rightarrow HO_2} = \frac{S_{RO_x} - S_{HO_x} + S_{OH}}{S_{OH_0} \cdot C_{OH+VOC} \cdot C_{HO_2 \rightarrow OH}} = \frac{S_{RO_x} - S_{HO_x} + S_{OH}}{(S_{HO_x} - S_{OH}) \cdot C_{OH+VOC}} \quad (11)$$

18 Because this method cannot distinguish between the different peroxy radicals that could be produced from each
 19 OH + VOC reaction, the measured conversion efficiency reflects the average conversion efficiency of all peroxy
 20 radicals for a given VOC.

21 3 Results

22 The pressure and flow conditions for the three campaigns conducted with the IU LIF-FAGE instrument are
 23 summarized in Table 1. For each characterization, the flow rate of NO addition was kept constant at 1 sccm in



1 order to determine the impact of the different operating conditions on the measured RO₂-to-HO₂ conversion
2 efficiencies. This is the NO flow rate used during the MCMA-2006, CABINEX and CalNex campaigns, and
3 resulted in HO₂-to-OH conversion efficiencies that were similar to that measured during both the CABINEX and
4 the CalNex campaigns. However, the measured HO₂-to-OH conversion efficiency for the MCMA-2006 campaign
5 configuration in these experiments was approximately 20% lower than that previously reported (Dusanter et al.,
6 2008; 2009a). The reason for this discrepancy is unclear, and may indicate problems in precisely recreating the
7 flow conditions during this campaign in these laboratory experiments. In addition, the NO flow rate was varied
8 during MCMA-2006 in order to maximize the HO₂-to-OH conversion efficiency and to quantify the photolytic
9 interference associated with high NO concentrations in the detection cell. Thus is possible that the actual flow rate
10 used to maximize the conversion efficiency was slightly greater than the 1 sccm reported. As a result, the
11 conversion efficiencies measured in this study for the MCMA-2006 configuration may represent a lower limit to
12 the actual conversion efficiencies during the campaign.

13 The RO₂ conversion efficiency into HO₂ ($f_{\text{RO}_2 \rightarrow \text{HO}_2}$) measured for the inlet conditions for the MCMA
14 2006, CABINEX, and CalNex campaigns are summarized in Table 2 and represent the results of several
15 experiments similar to those illustrated in Fig. 2, with the uncertainty representing one standard error of the mean
16 of the measurements. The largest RO₂ interference was observed for the CalNex inlet conditions where alkenes
17 produced interferences ranging from $83 \pm 7\%$ for isoprene-based peroxy radicals to $96 \pm 6\%$ for
18 tetramethylethylene (TME)-based peroxy radicals, while the conversion efficiency of aromatic, aldehydes, and
19 ketone compounds ranged from $54 \pm 4\%$ for methacrolein (MACR) to $91 \pm 4\%$ for methyl vinyl ketone (MVK).
20 The RO₂ to HO₂ conversion efficiency of a number of alkanes ranged from an average measured value of $15 \pm$
21 3% for propane-based peroxy radicals to $62 \pm 4\%$ for octane-based peroxy radicals, with the RO₂ to HO₂
22 conversion efficiency increasing with the carbon number. The inlet configuration and conditions used during the
23 MCMA 2006 campaign generally resulted in lower RO₂ interferences likely due to the higher flow rate (and
24 shorter reaction time) in the detection cell and the lower NO concentration, although the measured conversion
25 efficiency was found to be somewhat greater for some VOCs. Under these inlet conditions the RO₂ to HO₂
26 conversion efficiency for propane-based peroxy radicals was measured to be $22 \pm 11\%$ while the conversion
27 efficiency for octane-based peroxy radicals was $30 \pm 5\%$. Because the CABINEX campaign occurred in a remote
28 forested environment, measurements of the RO₂-to-HO₂ conversion efficiency focused on characterizing
29 interferences from peroxy radicals produced from isoprene and its oxidation products (MVK and MACR), as
30 isoprene peroxy radicals were predicted to contribute to more than 80% of the total RO₂ concentration during the
31 campaign (Griffith et al., 2013). The inlet and instrumental configuration during CABINEX resulted in a higher



1 pressure and slower sampling rate compared to the MCMA 2006 configuration. For this instrumental
2 configuration, the RO₂-to-HO₂ conversion efficiency was found to be 91 ± 5% for isoprene-based peroxy radicals,
3 while the conversion efficiencies for MVK and MACR were found to be 62 ± 5% and 30 ± 7%, respectively.

4 These observations are consistent with results reported for other FAGE instruments (Fuchs et al., 2011;
5 Whalley et al., 2011), and assumes that the photolysis of each VOC does not contribute to the production of
6 radicals in these experiment. However, tests to determine whether photolysis of the various VOCs resulted in the
7 formation of HO_x radicals in the absence of water vapor revealed that the photolysis of methyl vinyl ketone
8 (MVK), methacrolein (MACR), methyl ethyl ketone (MEK), and toluene can lead to the production of HO_x
9 radicals. The radical signals from the photolysis of methacrolein, and toluene were small and negligible relative
10 to the total HO_x signal produced from the photolysis of water. However, the signal from the photolysis of MVK
11 and MEK during these tests was significant and could interfere with the measurements of the RO₂-to-HO₂
12 conversion efficiency. These results are in contrast to that reported by Fuchs et al. (2011), who found that the
13 photolysis of VOCs during similar tests in dry air did not produce any radicals. The interference from the radicals
14 produced from the photolysis of MVK and MEK would result in higher apparent conversion efficiencies, and
15 could contribute to the higher RO₂-to-HO₂ conversion efficiency reported here for MVK compared to that reported
16 by Fuchs et al. (2011).

17 As previously observed, the RO₂-to-HO₂ conversion efficiency of alkene-based β-hydroxyalkyl peroxy
18 radicals was found to be greater than the conversion efficiency of alkane-based alkyl peroxy radicals (Fuchs et
19 al., 2011). As discussed above, this is due to due to the ability of the β-hydroxyalkoxy radicals produced from the
20 RO₂ + NO reaction to rapidly decompose to form a hydroxyalkyl radical that can reacts rapidly with O₂ in the
21 FAGE detection cell leading to the production of a carbonyl compound and HO₂. However, the ability of large
22 alkoxy radicals to rapidly isomerize and decompose also results in a rapid production of HO₂ radicals and a larger
23 conversion efficiency.

24 In general, reducing the reaction time in the IU-FAGE instrument reduces the conversion of these peroxy
25 radicals to HO₂, as illustrated by the reduced conversion efficiencies between the CalNex and MCMA operating
26 conditions for the majority of the VOCs tested. However, the measured conversion efficiencies of some of the
27 tested VOCs did not always display this behavior and the reasons for the discrepancies are unclear. For example,
28 the conversion efficiency for ethene peroxy radicals was lower for the CalNex configuration compared to the
29 CABINEX and MCMA configurations even though the overall flow rate was slower for the CalNex configuration.
30 However, the HO₂-to-OH conversion efficiency was also lower for this inlet configuration, suggesting that
31 reaction time may not be the only factor limiting the conversion efficiency under these instrument conditions.



1 Similarly, the conversion efficiency of MVK and MACR measured for the CABINEX instrument configuration
2 was lower than that measured for the MCMA inlet configuration, even though the overall slower flow rate in the
3 CABINEX configuration leads to a longer reaction time in the IU-FAGE detection cell. This may suggest that the
4 chemistry of peroxy radicals produced from the OH-initiated oxidation of MVK and MACR is different than that
5 of the peroxy radicals produced from the OH-initiated oxidation of alkenes and alkanes (Fuchs et al., 2011).

6 **4 Discussion**

7 **4.1 RO₂ Radical Concentrations during MCMA 2006**

8 The previous analysis of the HO₂ radical concentrations during the Mexico City Metropolitan Area (MCMA)
9 2006 did not take into account interferences from RO₂ radicals (Dusanter et al., 2009b). As discussed above, the
10 instrumental conditions during MCMA-2006 resulted in the conversion of a fraction of RO₂ radicals to HO₂,
11 resulting in the measurements reflecting HO₂* = HO₂ + αRO₂ and overestimating the actual HO₂ concentrations.
12 To determine the fraction (α) of RO₂ radicals likely detected during the HO₂ measurements, the RO₂ radical
13 concentrations during MCMA-2006 that were previously modeled using the Regional Atmospheric Chemistry
14 Mechanism (RACM) were used to calculate the modeled HO₂* concentrations (Dusanter et al., 2009b).

15 As discussed in Dusanter et al. (2009b), the RACM model is a condensed chemical mechanism that
16 describes the gas-phase oxidation of 17 inorganic and 32 organic species. Kinetic parameters for the reactions of
17 OH, O₃ and NO₃ with inorganic species and for reactions involving organic species treated explicitly in RACM
18 (methane, ethane, ethene, formaldehyde, glyoxal, methyl peroxide and isoprene) were updated using the JPL
19 database (Sanders et al., 2006). Rate constants and branching ratios for OH, O₃ and NO₃ reactions with surrogate
20 species were used as described in the RACM model (Stockwell et al., 1997). Heterogeneous chemistry, such as
21 the incorporation of trace gases into aerosols, was not included.

22 The peroxy radical fractions calculated by the model are illustrated in Fig. 4 for 9 am, 12 pm, 6pm (local
23 times) and the overall diurnal average. Alkane-based peroxy radicals (red shades) include methyl peroxy (RACM
24 category CH₃O₂), ethyl peroxy (ETHP), peroxy radicals formed from the oxidation of alkanes, esters, and alkynes
25 exhibiting OH rate constants lower than $3.4 \times 10^{-12} \text{ cm}^3 \text{ molecule}^{-1} \text{ s}^{-1}$ (HC3P), peroxy radicals formed from
26 alkanes, esters, and alkynes characterized by OH rate constants ranging from 3.4×10^{-12} to $6.8 \times 10^{-12} \text{ cm}^3$
27 $\text{molecule}^{-1} \text{ s}^{-1}$ (HC5P), and peroxy radicals formed from alkanes, esters, and alkynes whose OH rate constants are
28 larger than $6.8 \times 10^{-12} \text{ cm}^3 \text{ molecule}^{-1} \text{ s}^{-1}$ (HC8P). Alkene-based peroxy radicals (blue shades) include peroxy
29 radicals from the oxidation of ethene (ETEP), external olefins (OLTP), internal olefins (OLIP), isoprene (ISOP),



1 and from α -pinene and other cyclic terpenes with one double bond (APIP). Aromatic peroxy radicals (green
2 shades) include species produced during the oxidation of toluene (TOLP), xylenes (XYLP), and cresol (CSLP).
3 The carbonyl-based peroxy radicals (grey shades) include saturated (ACO3) and unsaturated (TCO3) acyl peroxy
4 radicals.

5 The total average modeled RO₂ concentration from 9:00 am to 6:00 pm consisted of 54% alkane-based,
6 27% alkene-based, and 14% aromatic-based peroxy radicals (Fig. 4). On average, the modeled composition of
7 peroxy radicals was relatively constant throughout the day during the MCMA campaign. The modeled relative
8 contribution of aromatic-based peroxy radicals was greater in the morning, consistent with the observed elevated
9 concentrations of benzene and toluene during the morning hours (Dusanter et al., 2009b).

10 **4.2 Implications of RO₂ interferences for HO₂ measurements during MCMA 2006**

11 The modeled diurnal average concentrations of total RO₂ radicals during MCMA is shown in Fig. 5, along with
12 the modeled HO₂ concentrations and the measured HO₂* concentrations. As discussed in Dusanter et al. (2009b),
13 the modeled HO₂ concentrations were in good agreement with the measurements during the afternoon but the
14 model underestimated the measured HO₂ concentrations during the morning hours by a factor of approximately 2
15 to 5. However, these conclusions were based on the assumption that the measured HO₂ concentrations were free
16 from interferences and could be compared to the modeled HO₂ concentrations. Based on the conversion
17 efficiencies reported for RO₂ radicals in the present study, it is clear that the MCMA measurements represent an
18 upper limit to the actual HO₂ concentrations and should be compared to the modeled HO₂* = HO₂ + α RO₂
19 concentrations.

20 The RACM modeled HO₂* concentrations were calculated by applying the measured RO₂-to-HO₂
21 conversion efficiencies for the instrumental conditions reported in Table 2 for MCMA-2006 using Eq. 12:

$$\begin{aligned} 22 \quad HO_2^* = HO_2 + & (0.84 \cdot ISOP + 0.68 \cdot OLIP + 0.68 \cdot OLTP + 0.86 \cdot ETEP + 0.32 \cdot TOLP + 0.32 \cdot XYLP + \\ 23 \quad & 0.32 \cdot CSLP + 0.72 \cdot APIP + 0.22 \cdot HC3P + 0.22 \cdot HC5P + 0.30 \cdot HC8P + 0.05 \cdot CH3O2 + 0.07 \cdot ETHP \\ 24 \quad & + 0.32 \cdot ACO3 + 0.32 \cdot TCO3 + 0.72 \cdot KETP \end{aligned} \quad (12)$$

25 The contribution for isoprene peroxy radicals (ISOP), ethene peroxy radicals (ETEP), and toluene peroxy radicals
26 (TOLP) were taken directly from Table 2. The average RO₂-to-HO₂ conversion efficiency for *trans*-2-butene and
27 tetramethylethylene-based peroxy radicals was used for the conversion efficiency of peroxy radicals from internal
28 olefins (OLIP), and external olefins (OLTP), while the conversion efficiency for *trans*-2-butene was used for the
29 conversion efficiency for α -pinene and other cyclic terpene peroxy radicals (APIP). The measured conversion



1 efficiency for toluene-based peroxy radicals was used to represent the conversion efficiency for xylene (XYLP)
2 and cresol (CSLP) peroxy radicals. The conversion efficiency of methacrolein-based peroxy radicals was used to
3 represent the conversion efficiency of acetyl peroxy and higher saturated acyl peroxy radicals (ACO3) as well as
4 unsaturated acyl peroxy radicals (TCO3), while the conversion efficiency of methyl vinyl ketone-based peroxy
5 radicals was used to represent the efficiency of ketone-based peroxy radicals (KETP).

6 The overall average contribution of peroxy radicals to the modeled HO_2^* and the relative contribution of
7 each RACM peroxy radical category to the RO_2 interference are shown in Fig. 6. Because the NO flow rate used
8 in characterizing the conversion efficiencies in Table 2 was generally lower than the flow rates used during the
9 campaign, the relative peroxy radical contributions illustrated in this figure are likely lower limits to the actual
10 contribution during the campaign, as the HO_2 -to-OH conversion efficiency of 80% in these experiments was
11 approximately 20% lower than the conversion efficiency measured during the campaign (Dusanter et al., 2008;
12 Dusanter et al., 2009a).

13 On average, RO_2 radicals contributed to approximately 35% of the total modeled HO_2^* (Fig. 6). While
14 alkanes compose the majority of the modeled peroxy radicals, they only contributed to about 29% of the RO_2
15 interference, while alkenes contributed to approximately 51% to the interference. The contribution of RO_2 radicals
16 to the measured HO_2^* concentrations in this environment is in contrast to measurements in forested environments
17 where the OH reactivity is dominated by isoprene and other unsaturated biogenic emissions. In these
18 environments, isoprene and other biogenic hydroxyl alkyl peroxy radicals can be the dominant peroxy radicals
19 and can make a significant contribution to the measured HO_2^* concentrations due to their high conversion
20 efficiency to HO_2 in the FAGE detection cell (Table 2). For example, during the CABINEX campaign in a northern
21 Michigan forest, isoprene peroxy radicals were modeled to be the dominant peroxy radical in this environment,
22 contributing to approximately 50% of the modeled HO_2^* concentrations during the daytime (Griffith et al., 2013).
23 As a result, previous measurements of HO_2 in these environments by LIF-FAGE or other chemical conversion
24 techniques are likely influenced by an interference from β -hydroxyalkyl peroxy radicals such as those produced
25 by the OH-initiated oxidation of isoprene and other biogenic emissions.

26 The diurnal average modeled HO_2^* concentrations for the MCMA-2006 campaign are also shown in Fig.
27 5. As can be seen in this figure, the model overestimates the measured HO_2^* by approximately 35% between
28 12:00 and 17:00 CST, although the modeled results are generally close to the upper bound of the calibration
29 accuracy (36%, 2σ) (Dusanter et al., 2009b). As discussed above, the modeled HO_2^* is likely a lower limit given
30 that the RO_2 -to- HO_2 conversion efficiencies during the campaign may be greater than shown in Table 2 due to the
31 higher NO flows used during the campaign. Although, the measured HO_2^* are still likely to be within the overall



1 uncertainty of the model, which was estimated to be approximately a factor of 1.7 (Dusanter et al., 2009b), these
2 results suggest that the model likely overestimates the measured concentrations during the afternoon.

3 These results are in contrast to the results from the CalNex campaign, where the simulations using the
4 RACM2 model tended to underestimate the measured HO₂* concentrations during the week, when NO mixing
5 ratios were greater than 4 ppb (Griffith et al., 2016). The reason for this difference between the campaigns is
6 unclear, but may be related to the relative concentrations of dicarbonyl species and their treatment in the RACM
7 and RACM2 models. Dusanter et al. (2009b) demonstrated that the RACM model results for MCMA-2006 were
8 highly sensitive to the concentrations of dicarbonyl species in the model, with the model significantly
9 overpredicting the concentration of HO_x radicals when unmeasured concentrations of these species were not
10 constrained. Daytime average measured glyoxal mixing ratios during MCMA-2006 were approximately 0.4 ppb
11 (Dusanter et al., 2009b), which were greater than the maximum daytime mixing ratios of 0.16 ppb during CalNex
12 (Washenfelder et al., 2011), suggesting that the MCMA-2006 results may be more sensitive to the treatment of
13 dicarbonyl chemistry compared to CalNex. Additional analysis and modeling will be needed to resolve this issue.

14 While the model tends to overestimate the measured HO₂* concentrations during the afternoon, it
15 underestimates the measured HO₂* concentrations in the morning by a factor of 3 between 9-11 am. As discussed
16 in Dusanter et al. (2009b), this may suggest that a significant radical source may be missing from current
17 atmospheric models under polluted conditions. Dusanter et al. (2009b) also compared the measured HO₂*/OH
18 ratio to the RACM modeled HO₂/OH ratio and found that the model underpredicted the observed ratio, especially
19 under conditions where the mixing ratio of NO was greater than 5 ppb. At NO mixing ratios of 10 ppb, the model
20 underestimated the measured ratio by a factor of 2 (Dusanter et al., 2009b). However, comparing the measured
21 HO₂*/OH ratio to the modeled HO₂*/OH ratio improves the agreement even though the model tends to overpredict
22 both OH and HO₂* in the afternoon (Fig. 7). This may indicate that there is either a missing sink of HO_x radicals
23 in the model or a miscalculation of the relative rates of initiation and/or termination. At an NO mixing ratio of 10
24 ppb the modeled HO₂*/OH ratio is in good agreement with the measurements, although it still underestimates the
25 measured HO₂*/OH ratio at higher NO mixing ratios by as much as a factor of 4, and may also overestimate the
26 HO₂*/OH ratio for mixing ratios of NO less than 5 ppb by as much as a factor of 2 (Fig. 7). It is interesting to note
27 that a model underestimation of the total OH reactivity at high NO mixing ratios may contribute to this
28 discrepancy. Unfortunately, total OH reactivity was not measured during MCMA-2006 and the reliability of the
29 model to simulate it could not be assessed. Similar results were observed for the CalNex campaign (Griffith et al.,
30 2016), which included direct measurements of the total OH reactivity. Although accounting for the missing
31 reactivity in the analysis of the CalNex data improved the agreement between the measured and modeled



1 HO₂*/OH ratio, the model still underestimates the measured ratio at high mixing ratios of NO (Griffith et al.,
2 2016). These results suggest that our understanding of the radical propagation chemistry under high NO conditions
3 may be incomplete.

4 **5. Summary and Conclusions**

5 The RO₂ interference associated with measurements of HO₂ by the IU-FAGE instrument was
6 characterized for three different instrument configurations that were used in previous field campaigns (MCMA
7 2006, CABINEX 2009, and CalNex 2010). Similar to that reported for other LIF-FAGE instruments, the RO₂-to-
8 HO₂ conversion efficiency was highest for alkene- and aromatic-based RO₂ radicals, producing higher levels of
9 interference, while the conversion efficiency of alkane-based RO₂ radicals was less but increased with increasing
10 carbon number. In general, the conversion efficiency was higher for instrument configurations that involved
11 slower sampling flow rates and longer reaction times between the peroxy radicals and NO in the detection cell.

12 The similarities in the measured RO₂ conversion efficiencies reported here with those reported for other
13 LIF-FAGE instruments suggest that the main factor controlling the conversion efficiency is the rate of reaction of
14 RO₂ radicals with NO, and that increasing the efficiency of the conversion of HO₂ to OH will also increase the
15 RO₂-to-HO₂ conversion efficiency. Although the impact of differences in the characteristics of the low pressure
16 expansion in LIF-FAGE instruments cannot be ruled out, these results suggest that the interferences reported here
17 associated with measurements of HO₂ are likely similar for all instruments that measure HO₂ by chemical
18 conversion through reaction with NO. Previous measurements of HO₂ radicals by instruments using this method
19 were likely influenced by the conversion of RO₂ radicals, with measurements of HO₂ in forested environments
20 likely influenced by interferences from peroxy radicals derived from biogenic alkenes such as isoprene due to the
21 high RO₂-to-HO₂ conversion efficiencies of these radicals. Because of the lower conversion efficiencies of alkane-
22 based peroxy radicals, the impact on previous measurements in urban areas will depend on the relative
23 concentrations of alkanes versus alkenes and aromatics contributing to the overall pool of peroxy radicals in these
24 environments.

25 While this interference was taken into account to investigate the radical chemistry during CABINEX
26 (Griffith et al., 2013) and CalNex (Griffith et al., 2016), this issue was not known when the radical measurements
27 from the MCMA-2006 field campaign were published (Dusanter et al., 2009b). An analysis of the impact of this
28 interference on the results for the MCMA-2006 campaign suggests that the RO₂ radical contribution to the
29 measured HO₂* concentration was approximately 35% based on the RACM modeled RO₂ concentrations. Taking



1 this interference into account, the resulting modeled HO₂* concentrations were generally greater than the
2 measured concentrations by 35% during the afternoon, although the model results were within the calibration
3 uncertainty of the measurements (36% at 2σ). Given that the modeled HO₂* concentrations likely reflect a lower
4 limit to the interference during the campaign these results suggest that the model likely overestimates the measured
5 concentrations during the afternoon. However, the model still underestimates the HO₂* concentration by a factor
6 of 3 in the morning, suggesting that the model may be missing an important radical source in the morning.
7 Although the measured HO₂*/OH ratio was in better agreement with the modeled HO₂*/OH ratio compared to the
8 modeled HO₂/OH ratio, the model still significantly underestimates the HO₂*/OH ratio by up to a factor of 4 for
9 NO mixing ratios greater than 10 ppb, suggesting that our understanding of radical propagation under these
10 conditions is still incomplete.

11 Future measurements of peroxy radicals by the IU-FAGE instrument will involve measurements at lower
12 NO concentrations to minimize the RO₂-to-HO₂ conversion efficiency. Recent experiments have demonstrated
13 that at an HO₂-to-OH conversion efficiency of approximately 17%, the conversion efficiency of isoprene-based
14 peroxy radicals is less than 10%. Even at this low HO₂-to-OH conversion efficiency, the resulting HO₂ signals are
15 still significantly greater than the limit of detection of the instrument, allowing for measurements of ambient HO₂
16 concentrations without interferences from RO₂ radicals.

Acknowledgements. This work was supported by grants from the National Science Foundation (AGS-1104880 and AGS-1440834) and the National Aeronautics and Space Administration (NNX12AE55G). We would also like to thank Stephen Griffith for his helpful insights during the early stages of this project and Jennifer Liljegren for experimental assistance.



References

- Cantrell, C. A., Zimmer, A., and Tyndall, G. S.: Absorption cross sections for water vapor from 183 to 193 nm, *Geophysical Research Letters*, 24, 2195-2198, 1997.
- Carslaw, N., Creasey, D. J., Harrison, D., Heard, D. E., Hunter, M. C., Jacobs, P. J., Jenkin, M. E., Lee, J. D., Lewis, A. C., Pilling, M. J., Saunders, S. M., and Seakins, P. W.: OH and HO₂ radical chemistry in a forested region of north-western Greece, *Atmospheric Environment*, 35, 4725-4737, 2001.
- Chen, S., Ren, X., Mao, J., Chen, Z., Brune, W. H., Lefer, B., Rappenglück, B., Flynn, J., Olson, J., and Crawford, J. H.: A comparison of chemical mechanisms based on TRAMP-2006 field data, *Atmospheric Environment*, 44, 4116-4125, 2010.
- Creasey, D. J., Heard, D. E., and Lee, J. D.: Absorption cross-section measurements of water vapour and oxygen at 185 nm. Implications for the calibration of field instruments to measure OH, HO₂ and RO₂ radicals, *Geophysical Research Letters*, 27, 1651-1654, 2000.
- Creasey, D. J., Heard, D. E., and Lee, J. D.: Eastern Atlantic Spring Experiment 1997 (EASE97) 1. Measurements of OH and HO₂ concentrations at Mace Head, Ireland, *Journal of Geophysical Research: Atmospheres*, 107, 4091, [4010.1029/2001JD000892](https://doi.org/10.1029/2001JD000892), 2002.
- Czader, B. H., Li, X., and Rappenglueck, B.: CMAQ modeling and analysis of radicals, radical precursors, and chemical transformations, *J. Geophys. Res.*, 118, 11,376-311,387, 2013.
- Dusanter, S., Vimal, D., and Stevens, P. S.: Technical note: Measuring tropospheric OH and HO₂ by laser-induced fluorescence at low pressure. A comparison of calibration techniques, *Atmos. Chem. Phys.*, 8, 321-340, 2008.
- Dusanter, S., Vimal, D., Stevens, P. S., Volkamer, R., and Molina, L. T.: Measurements of OH and HO₂ concentrations during the MCMA-2006 field campaign – Part 1: Deployment of the Indiana University laser-induced fluorescence instrument, *Atmos. Chem. Phys.*, 9, 1665-1685, 2009a.
- Dusanter, S., Vimal, D., Stevens, P. S., Volkamer, R., Molina, L. T., Baker, A., Meinardi, S., Blake, D., Sheehy, P., Merten, A., Zhang, R., Zheng, J., Fortner, E. C., Junkermann, W., Dubey, M., Rahn, T., Eichinger, B., Lewandowski, P., Prueger, J., and Holder, H.: Measurements of OH and HO₂ concentrations during the MCMA-2006 field campaign – Part 2: Model comparison and radical budget, *Atmos. Chem. Phys.*, 9, 6655-6675, 2009b.
- Emmerson, K. M., Carslaw, N., Carpenter, L. J., Heard, D. E., Lee, J. D., and Pilling, M. J.: Urban Atmospheric Chemistry During the PUMA Campaign 1: Comparison of Modelled OH and HO₂ Concentrations with Measurements, *J Atmos Chem*, 52, 143-164, 2005.
- Emmerson, K. M., Carslaw, N., Carslaw, D. C., Lee, J. D., McFiggans, G., Bloss, W. J., Gravestock, T., Heard, D. E., Hopkins, J., Ingham, T., Pilling, M. J., Smith, S. C., Jacob, M., and Monks, P. S.: Free radical modelling studies during the UK TORCH Campaign in Summer 2003, *Atmos. Chem. Phys.*, 7, 167-181, 2007.
- Fuchs, H., Brauers, T., Dorn, H. P., Harder, H., Häsel, R., Hofzumahaus, A., Holland, F., Kanaya, Y., Kajii, Y., Kubistin, D., Lou, S., Martinez, M., Miyamoto, K., Nishida, S., Rudolf, M., Schlosser, E., Wahner, A., Yoshino, A., and Schurath, U.: Technical Note: Formal blind intercomparison of HO₂ measurements in the atmosphere simulation chamber SAPHIR during the HOxComp campaign, *Atmos. Chem. Phys.*, 10, 12233-12250, 2010.
- Fuchs, H., Bohn, B., Hofzumahaus, A., Holland, F., Lu, K. D., Nehr, S., Rohrer, F., and Wahner, A.: Detection of HO₂ by laser-induced fluorescence: calibration and interferences from RO₂ radicals, *Atmos. Meas. Tech.*, 4, 1209-1225, 2011.
- George, L. A., Hard, T. M., and O'Brien, R. J.: Measurement of free radicals OH and HO₂ in Los Angeles smog, *Journal of Geophysical Research: Atmospheres*, 104, 11643-11655, 1999.



- Griffith, S. M., Hansen, R. F., Dusanter, S., Stevens, P. S., Alaghmand, M., Bertman, S. B., Carroll, M. A., Erickson, M., Galloway, M., Grossberg, N., Hottle, J., Hou, J., Jobson, B. T., Kammrath, A., Keutsch, F. N., Lefer, B. L., Mielke, L. H., O'Brien, A., Shepson, P. B., Thurlow, M., Wallace, W., Zhang, N., and Zhou, X. L.: OH and HO₂ radical chemistry during PROPHET 2008 and CABINEX 2009 - Part 1: Measurements and model comparison, *Atmos. Chem. Phys.*, 13, 5403-5423, 2013.
- Griffith, S. M., Hansen, R. F., Dusanter, S., Michoud, V., Gilman, J. B., Kuster, W. C., Veres, P. R., Graus, M., de Gouw, J. A., Roberts, J., Young, C., Washenfelder, R., Brown, S. S., Thalman, R., Waxman, E., Volkamer, R., Tsai, C., Stutz, J., Flynn, J. H., Grossberg, N., Lefer, B., Alvarez, S. L., Rappenglueck, B., Mielke, L. H., Osthoff, H. D., and Stevens, P. S.: Measurements of hydroxyl and hydroperoxy radicals during CalNex-LA: Model comparisons and radical budgets, *Journal of Geophysical Research: Atmospheres*, 121, 4211-4232, 2016.
- Heard, D. E., and Pilling, M. J.: Measurement of OH and HO₂ in the troposphere, *Chemical Reviews*, 103, 5163-5198, 2003.
- Hens, K., Novelli, A., Martinez, M., Auld, J., Axinte, R., Bohn, B., Fischer, H., Keronen, P., Kubistin, D., Nölscher, A. C., Oswald, R., Paasonen, P., Petäjä, T., Regelin, E., Sander, R., Sinha, V., Sipilä, M., Taraborrelli, D., Tatum Ernest, C., Williams, J., Lelieveld, J., and Harder, H.: Observation and modelling of HO_x radicals in a boreal forest, *Atmos. Chem. Phys.*, 14, 8723-8747, 2014.
- Hofzumahaus, A., Brauers, T., Aschmutat, U., Brandenburger, U., Dorn, H. P., Hausmann, M., Heßling, M., Holland, F., Plass-Dülmer, C., Sedlacek, M., Weber, M., and Ehhalt, D. H.: Reply to "Comment on 'The measurement of tropospheric OH radicals by laser-induced fluorescence spectroscopy during the POPCORN field campaign' by Hofzumahaus et al. and 'Intercomparison of tropospheric OH radical measurements by multiple folded long-path laser absorption and laser induced fluorescence' by Brauers et al.", *Geophysical Research Letters*, 24, 3039-3040, 1997.
- Holland, F., Hofzumahaus, A., Schäfer, J., Kraus, A., and Pätz, H.-W.: Measurements of OH and HO₂ radical concentrations and photolysis frequencies during BERLIOZ, *Journal of Geophysical Research: Atmospheres*, 108, 8246, doi:10.1029/2001JD001393, 2003.
- Kanaya, Y., Sadanaga, Y., Hirokawa, J., Kajii, Y., and Akimoto, H.: Development of a Ground-Based LIF Instrument for Measuring HO_x Radicals: Instrumentation and Calibrations, *J Atmos Chem*, 38, 73-110, 2001.
- Kanaya, Y., Cao, R., Akimoto, H., Fukuda, M., Komazaki, Y., Yokouchi, Y., Koike, M., Tanimoto, H., Takegawa, N., and Kondo, Y.: Urban photochemistry in central Tokyo: 1. Observed and modeled OH and HO₂ radical concentrations during the winter and summer of 2004, *Journal of Geophysical Research: Atmospheres*, 112, doi:10.1029/2007JD008670, 2007a.
- Kanaya, Y., Cao, R., Kato, S., Miyakawa, Y., Kajii, Y., Tanimoto, H., Yokouchi, Y., Mochida, M., Kawamura, K., and Akimoto, H.: Chemistry of OH and HO₂ radicals observed at Rishiri Island, Japan, in September 2003: Missing daytime sink of HO₂ and positive nighttime correlations with monoterpenes, *Journal of Geophysical Research: Atmospheres*, 112, doi:10.1029/2006JD007987, 2007b.
- Kanaya, Y., Hofzumahaus, A., Dorn, H. P., Brauers, T., Fuchs, H., Holland, F., Rohrer, F., Bohn, B., Tillmann, R., Wegener, R., Wahner, A., Kajii, Y., Miyamoto, K., Nishida, S., Watanabe, K., Yoshino, A., Kubistin, D., Martinez, M., Rudolf, M., Harder, H., Berresheim, H., Elste, T., Plass-Dülmer, C., Stange, G., Kleffmann, J., Elshorbany, Y., and Schurath, U.: Comparisons of observed and modeled OH and HO₂ concentrations during the ambient measurement period of the HO_xComp field campaign, *Atmos. Chem. Phys.*, 12, 2567-2585, 2012.
- Kim, S., Wolfe, G. M., Mauldin, L., Cantrell, C., Guenther, A., Karl, T., Turnipseed, A., Greenberg, J., Hall, S. R., Ullmann, K., Apel, E., Hornbrook, R., Kajii, Y., Nakashima, Y., Keutsch, F. N., DiGangi, J. P., Henry, S. B., Kaser, L., Schnitzhofer, R., Graus, M., Hansel, A., Zheng, W., and Flocke, F. F.:



- Evaluation of HO_x sources and cycling using measurement-constrained model calculations in a 2-methyl-3-butene-2-ol (MBO) and monoterpene (MT) dominated ecosystem, *Atmos. Chem. Phys.*, 13, 2031-2044, 2013.
- Klotz, B., Sørensen, S., Barnes, I., Becker, K. H., Eitzkorn, T., Volkamer, R., Platt, U., Wirtz, K., and Martín-Reviejo, M.: Atmospheric Oxidation of Toluene in a Large-Volume Outdoor Photoreactor: In Situ Determination of Ring-Retaining Product Yields, *The Journal of Physical Chemistry A*, 102, 10289-10299, 1998.
- Konrad, S., Schmitz, T., Buers, H. J., Houben, N., Mannschreck, K., Mihelcic, D., Müsgen, P., Pätz, H. W., Holland, F., Hofzumahaus, A., Schäfer, H. J., Schröder, S., Volz-Thomas, A., Bächmann, K., Schlomski, S., Moortgat, G., and Großmann, D.: Hydrocarbon measurements at Pabstthum during the BERLIOZ campaign and modeling of free radicals, *J. Geophys. Res.*, 108, 8251, 2003.
- Kubistin, D., Harder, H., Martinez, M., Rudolf, M., Sander, R., Bozem, H., Eerdeken, G., Fischer, H., Gurk, C., Klüpfel, T., Königstedt, R., Parchatka, U., Schiller, C. L., Stickler, A., Taraborrelli, D., Williams, J., and Lelieveld, J.: Hydroxyl radicals in the tropical troposphere over the Suriname rainforest: comparison of measurements with the box model MECCA, *Atmos. Chem. Phys.*, 10, 9705-9728, 2010.
- Lanzendorf, E. J., Hanisco, T. F., Donahue, N. M., and Wennberg, P. O.: Comment on: "The measurement of tropospheric OH radicals by laser-induced fluorescence spectroscopy during the POPCORN Field Campaign" by Hofzumahaus et al. and "Intercomparison of tropospheric OH radical measurements by multiple folded long-path laser absorption and laser induced fluorescence" by Brauers et al, *Geophysical Research Letters*, 24, 3037-3038, 1997.
- Levy, H.: Photochemistry of the lower troposphere, *Planetary and Space Science*, 20, 919-935, 1972.
- Lu, K. D., Hofzumahaus, A., Holland, F., Bohn, B., Brauers, T., Fuchs, H., Hu, M., Häsel, R., Kita, K., Kondo, Y., Li, X., Lou, S. R., Oebel, A., Shao, M., Zeng, L. M., Wahner, A., Zhu, T., Zhang, Y. H., and Rohrer, F.: Missing OH source in a suburban environment near Beijing: observed and modelled OH and HO₂ concentrations in summer 2006, *Atmos. Chem. Phys.*, 13, 1057-1080, 2013.
- Mao, J., Ren, X., Zhang, L., Van Duin, D. M., Cohen, R. C., Park, J. H., Goldstein, A. H., Paulot, F., Beaver, M. R., Crouse, J. D., Wennberg, P. O., DiGangi, J. P., Henry, S. B., Keutsch, F. N., Park, C., Schade, G. W., Wolfe, G. M., Thornton, J. A., and Brune, W. H.: Insights into hydroxyl measurements and atmospheric oxidation in a California forest, *Atmos. Chem. Phys.*, 12, 8009-8020, 2012.
- Martinez, M., Harder, H., Kovacs, T. A., Simpas, J. B., Bassis, J., Leshner, R., Brune, W. H., Frost, G. J., Williams, E. J., Stroud, C. A., Jobson, B. T., Roberts, J. M., Hall, S. R., Shetter, R. E., Wert, B., Fried, A., Alicke, B., Stutz, J., Young, V. L., White, A. B., and Zamora, R. J.: OH and HO₂ concentrations, sources, and loss rates during the Southern Oxidants Study in Nashville, Tennessee, summer 1999, *Journal of Geophysical Research: Atmospheres*, 108, n/a-n/a, 2003.
- Michoud, V., Kukui, A., Camredon, M., Colomb, A., Borbon, A., Miet, K., Aumont, B., Beekmann, M., Durand-Jolibois, R., Perrier, S., Zapf, P., Siour, G., Ait-Helal, W., Locoge, N., Sauvage, S., Afif, C., Gros, V., Furger, M., Ancellet, G., and Doussin, J. F.: Radical budget analysis in a suburban European site during the MEGAPOLI summer field campaign, *Atmos. Chem. Phys.*, 12, 11951-11974, 2012.
- Nehr, S., Bohn, B., Fuchs, H., Hofzumahaus, A., and Wahner, A.: HO₂ formation from the OH + benzene reaction in the presence of O₂, *Physical Chemistry Chemical Physics*, 13, 10699-10708, 2011.
- Okabe, H.: Photochemistry of small molecules, John Wiley & Sons, New York, 1978.
- Ren, X., Harder, H., Martinez, M., Leshner, R. L., Oligier, A., Simpas, J. B., Brune, W. H., Schwab, J. J., Demerjian, K. L., He, Y., Zhou, X., and Gao, H.: OH and HO₂ Chemistry in the urban atmosphere of New York City, *Atmospheric Environment*, 37, 3639-3651, 2003.



- Ren, X., Brune, W., Cantrell, C., Edwards, G., Shirley, T., Metcalf, A., and Leshner, R.: Hydroxyl and Peroxy Radical Chemistry in a Rural Area of Central Pennsylvania: Observations and Model Comparisons, *J Atmos Chem*, 52, 231-257, 2005.
- Ren, X., Brune, W. H., Olinger, A., Metcalf, A. R., Simpas, J. B., Shirley, T., Schwab, J. J., Bai, C., Roychowdhury, U., Li, Y., Cai, C., Demerjian, K. L., He, Y., Zhou, X., Gao, H., and Hou, J.: OH, HO₂, and OH reactivity during the PMTACS–NY Whiteface Mountain 2002 campaign: Observations and model comparison, *Journal of Geophysical Research: Atmospheres*, 111, doi:10.1029/2005JD006126, 2006.
- Ren, X., van Duin, D., Cazorla, M., Chen, S., Mao, J., Zhang, L., Brune, W. H., Flynn, J. H., Grossberg, N., Lefter, B. L., Rappenglück, B., Wong, K. W., Tsai, C., Stutz, J., Dibb, J. E., Thomas Jobson, B., Luke, W. T., and Kelley, P.: Atmospheric oxidation chemistry and ozone production: Results from SHARP 2009 in Houston, Texas, *Journal of Geophysical Research: Atmospheres*, 118, 5770-5780, 2013.
- Rohrer, F., Lu, K., Hofzumahaus, A., Bohn, B., Brauers, T., Chang, C.-C., Fuchs, H., Haseler, R., Holland, F., Hu, M., Kita, K., Kondo, Y., Li, X., Lou, S., Oebel, A., Shao, M., Zeng, L., Zhu, T., Zhang, Y., and Wahner, A.: Maximum efficiency in the hydroxyl-radical-based self-cleansing of the troposphere, *Nature Geosci*, 7, 559-563, 2014.
- Sanders, S. P., Friedl, R. R., Golden, D. M., Kurylo, M. J., Moortgat, G. K., Wine, P. H., Ravishankara, A. R., Kolb, C. E., Molina, M. J., Finlayson-Pitts, B. J., Huie, R. E., and Orkin, V. L.: Chemical Kinetics and photochemical data for use in atmospheric studies, Evaluation Number 15, JPL Publications 06-2, 2006.
- Sheehy, P. M., Volkamer, R., Molina, L. T., and Molina, M. J.: Oxidative capacity of the Mexico City atmosphere – Part 2: A RO_x radical cycling perspective, *Atmos. Chem. Phys.*, 10, 6993-7008, 2010.
- Shirley, T. R., Brune, W. H., Ren, X., Mao, J., Leshner, R., Cardenas, B., Volkamer, R., Molina, L. T., Molina, M. J., Lamb, B., Velasco, E., Jobson, T., and Alexander, M.: Atmospheric oxidation in the Mexico City Metropolitan Area (MCMA) during April 2003, *Atmos. Chem. Phys.*, 6, 2753-2765, 2006.
- Stevens, P. S., Mather, J. H., and Brune, W. H.: Measurement of tropospheric OH and HO₂ by laser-induced fluorescence at low pressure, *J. Geophys. Res.*, 99, 3543-3557, 1994.
- Stockwell, W. R., Kirchner, F., Kuhn, M., and Seefeld, S.: A new mechanism for regional atmospheric chemistry modeling, *Journal of Geophysical Research: Atmospheres*, 102, 25847-25879, 1997.
- Tan, D., Faloon, I., Simpas, J. B., Brune, W., Shepson, P. B., Couch, T. L., Sumner, A. L., Carroll, M. A., Thornberry, T., Apel, E., Riemer, D., and Stockwell, W.: HO_x budgets in a deciduous forest: Results from the PROPHET summer 1998 campaign, *Journal of Geophysical Research: Atmospheres*, 106, 24407-24427, 2001.
- Washenfelder, R. A., Young, C. J., Brown, S. S., Angevine, W. M., Atlas, E. L., Blake, D. R., Bon, D. M., Cubison, M. J., de Gouw, J. A., Dusanter, S., Flynn, J., Gilman, J. B., Graus, M., Griffith, S., Grossberg, N., Hayes, P. L., Jimenez, J. L., Kuster, W. C., Lefter, B. L., Pollack, I. B., Ryerson, T. B., Stark, H., Stevens, P. S., and Trainer, M. K.: The glyoxal budget and its contribution to organic aerosol for Los Angeles, California, during CalNex 2010, *Journal of Geophysical Research: Atmospheres*, 116, doi:10.1029/2011JD016314, 2011.
- Whalley, L. K., Edwards, P. M., Furneaux, K. L., Goddard, A., Ingham, T., Evans, M. J., Stone, D., Hopkins, J. R., Jones, C. E., Karunaharan, A., Lee, J. D., Lewis, A. C., Monks, P. S., Moller, S. J., and Heard, D. E.: Quantifying the magnitude of a missing hydroxyl radical source in a tropical rainforest, *Atmos. Chem. Phys.*, 11, 7223-7233, 2011.
- Whalley, L. K., Blitz, M. A., Desservettaz, M., Seakins, P. W., and Heard, D. E.: Reporting the sensitivity of laser-induced fluorescence instruments used for HO₂ detection to an interference from RO₂ radicals and



introducing a novel approach that enables HO₂ and certain RO₂ types to be selectively measured,
Atmos. Meas. Tech., 6, 3425-3440, 2013.



Table 1. Configuration of the IU-FAGE instrument during various previous field campaigns.

	CalNex	CABINEX	MCMA-2006
Cell pressure (Torr)	4.1	7.5	5.4
Orifice diameter (mm/in)	0.64/0.025	1.02/0.04	1.02/0.04
Sample flow rate (SLPM)	3.4	8.5	10
NO (molecules/cm ³)	2.9×10^{13}	2.1×10^{13}	1.3×10^{13}



Table 2. Average measured $f_{\text{RO}_2 \rightarrow \text{HO}_2}$ for various alkenes and alkanes under different inlet conditions. Uncertainties represents the standard error of the mean from all individual experiments, with the number of experiments shown in parentheses.

Compounds	4 Torr @ 3.4 SLPM (CalNex)	7.5 Torr @ 8.5 SLPM (CABINEX)	5 Torr @ 10 SLPM (MCMA 2006)	Fuchs et al. ^a	Whalley et al. ^b
C(HO ₂ →OH)	0.67 ± 0.01 (67)	0.90 ± 0.02 (47)	0.80 ± 0.01 (81)	—	—
Isoprene	0.83 ± 0.07 (5)	0.91 ± 0.05 (9)	0.84 ± 0.05 (6)	0.79 ± 0.05	0.92 ± 0.04
MVK	0.91 ± 0.04 (10)	0.62 ± 0.05 (21)	0.72 ± 0.04 (15)	0.60 ± 0.06	—
MACR	0.54 ± 0.04 (4)	0.30 ± 0.07 (5)	0.32 ± 0.07 (11)	0.58 ± 0.17	—
MEK	0.57 ± 0.06 (6)	0.62 ± 0.01 (2)	0.51 ± 0.07 (9)	—	—
Ethene	0.65 ± 0.05 (18)	0.81 ± 0.06 (7)	0.86 ± 0.06 (9)	0.85 ± 0.05	1.00 ± 0.08
<i>trans</i> -2-butene	0.92 ± 0.04 (4)	—	0.72 ± 0.03 (6)	—	—
TME	0.96 ± 0.06 (2)	—	0.64 ± 0.06 (8)	—	—
Toluene	0.65 ± 0.07 (4)	—	0.32 ± 0.10 (6)	—	—
Propane	0.15 ± 0.03 (5)	—	0.22 ± 0.11 (2)	—	0.03 ± 0.01
n-butane	0.31 ± 0.03 (4)	0.30 ± 0.03 (3)	0.23 ± 0.05 (4)	—	0.18 ± 0.01
n-octane	0.62 ± 0.04 (5)	—	0.30 ± 0.05 (5)	—	—

^aFraction of conversion for RO₂ to HO₂ conversion for the Julich LIF instrument.(Fuchs et al., 2011)

^bConversion efficiencies of RO₂ to OH for the Leeds LIF instrument referenced to ethene (Whalley et al., 2013)

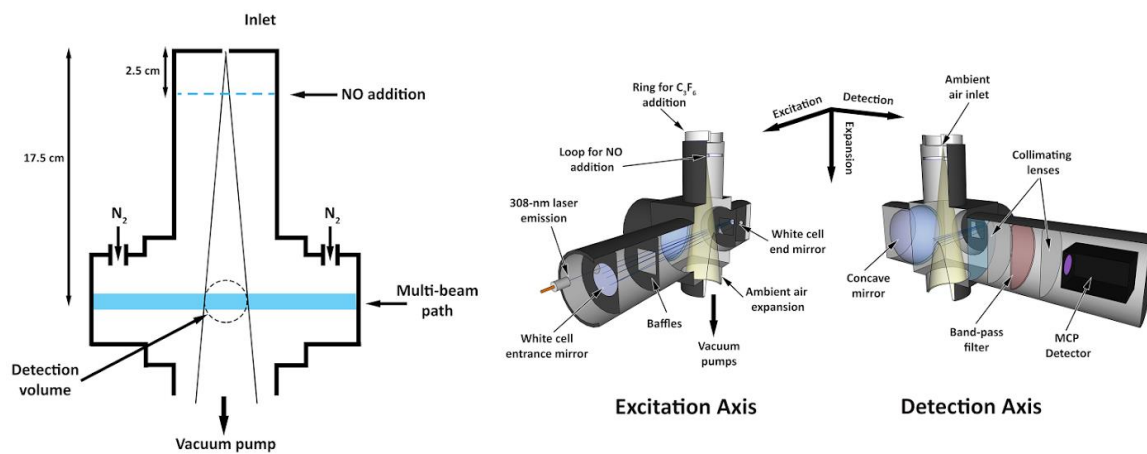


Figure 1. Indiana University LIF-FAGE cross section (left) and a schematic of the sampling/excitation axis and the sampling detection axis (right) (Dusanter et al., 2008)

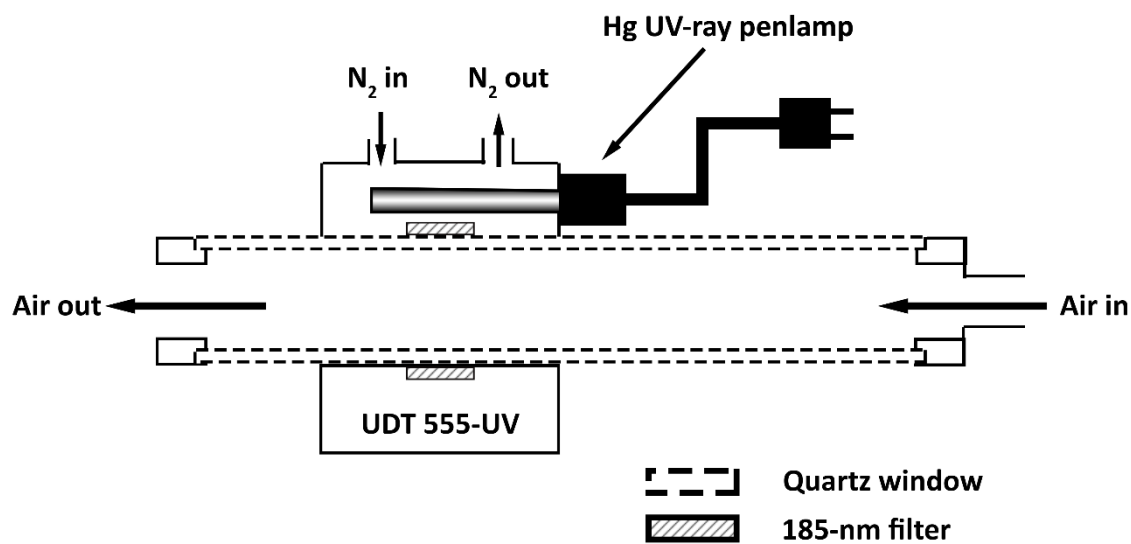


Figure 2. Cross-section of Indiana University calibration source for the IU-FAGE instrument

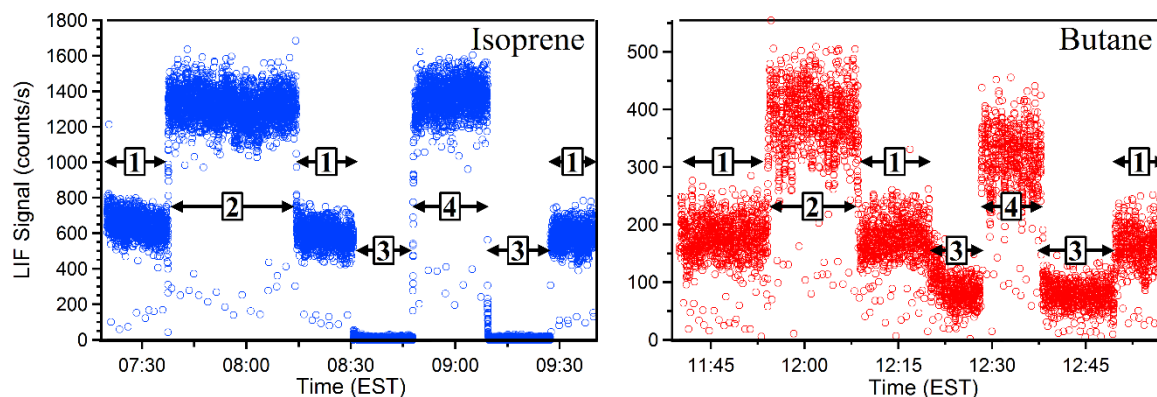


Figure 3. RO₂ interference measurement experiment for isoprene (left—with an OH reactivity of approximately 290 s⁻¹) and butane (right—with an OH reactivity of approximately 30 s⁻¹). The boxed numbers within the figure represents the various experimental modes: (1) S_{OH}, (2) S_{HOx} with internal NO addition, (3) S_{OH + VOC} with VOC added, (4) S_{ROx} with VOC added and internal NO addition.

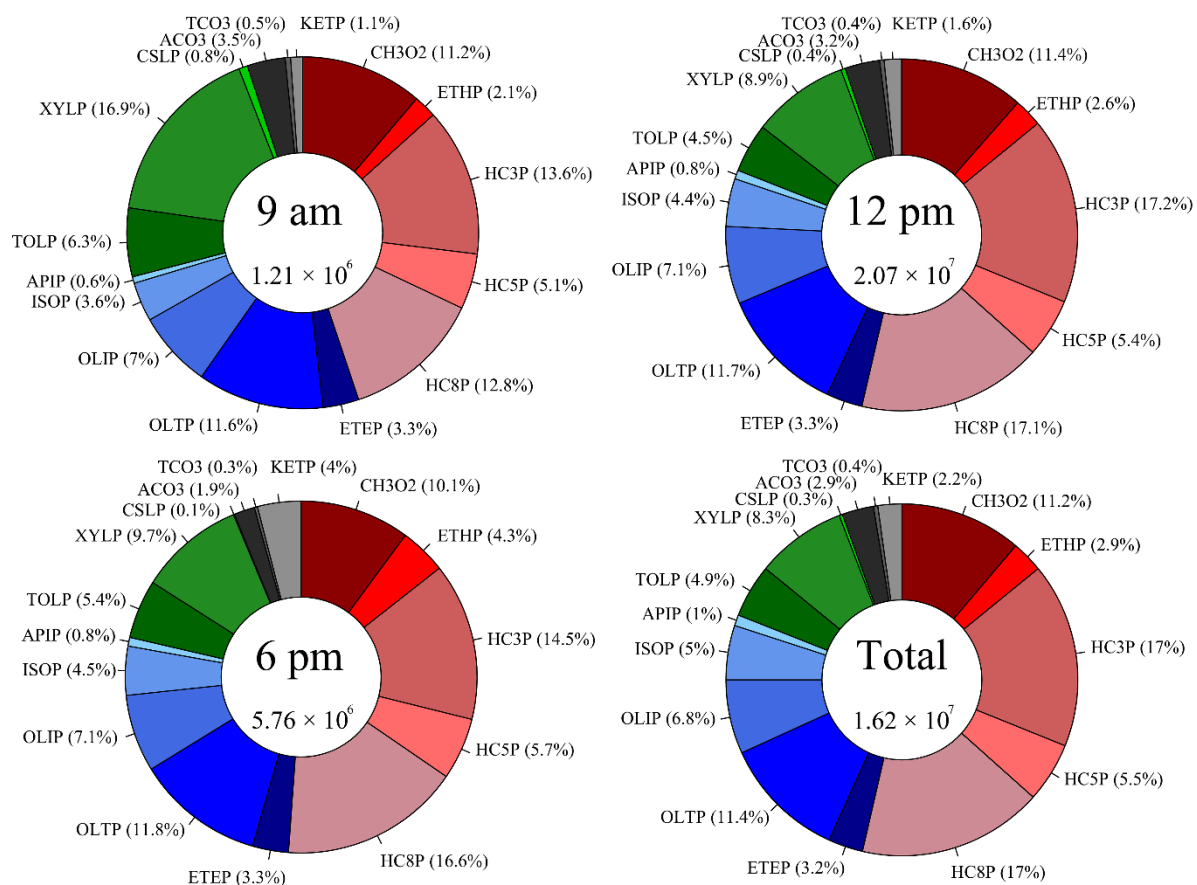


Figure 4. Modeled average peroxy radical contributions for the MCMA 2006 field campaign at 9:00 am (top left), 12:00 pm (top right), 6:00 pm (bottom left), and for the average campaign (bottom right). Shades of red represent alkanes, shades of blue represent alkenes, shades of green represent aromatics, and shades of grey represent acyl peroxy radicals.

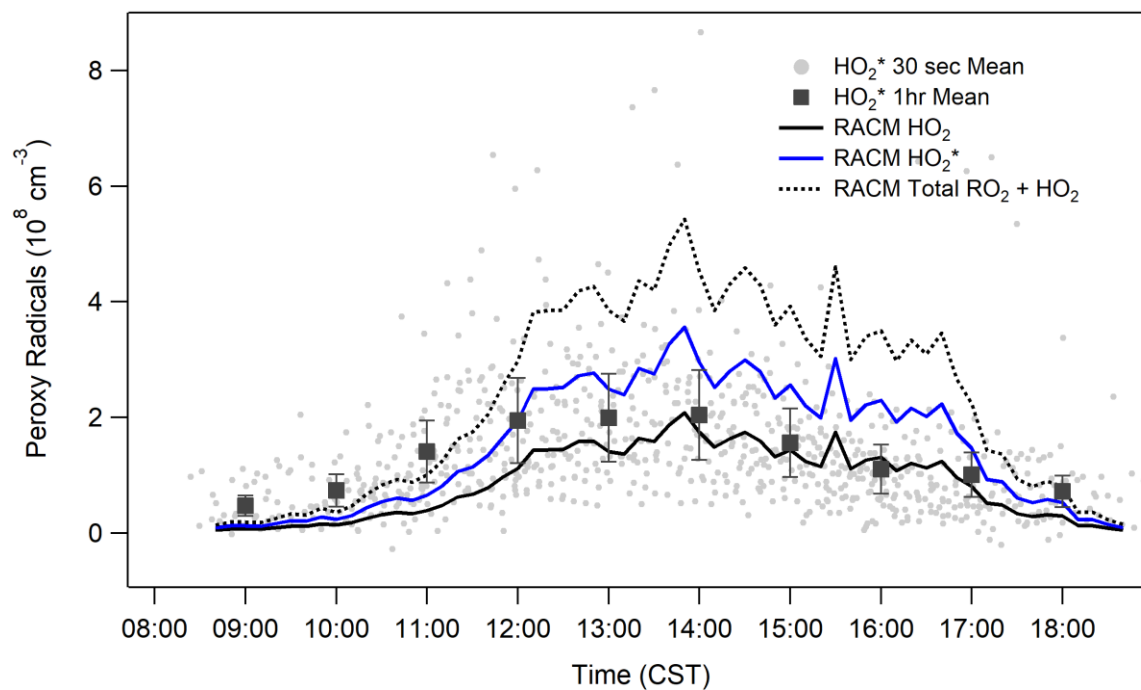


Figure 5. Diurnal average HO_2^* measurements from MCMA 2006. The grey solid circles are 30 sec averages and solid square symbols are binned 1 hour averages. The solid black line represents the RACM modeled HO_2 , the solid blue line represents the modeled HO_2^* , and the dotted black line represents the total modeled $\text{RO}_2 + \text{HO}_2$. The error bars reflect the calibration accuracy of the measurements ($\pm 36\%$, 2σ).

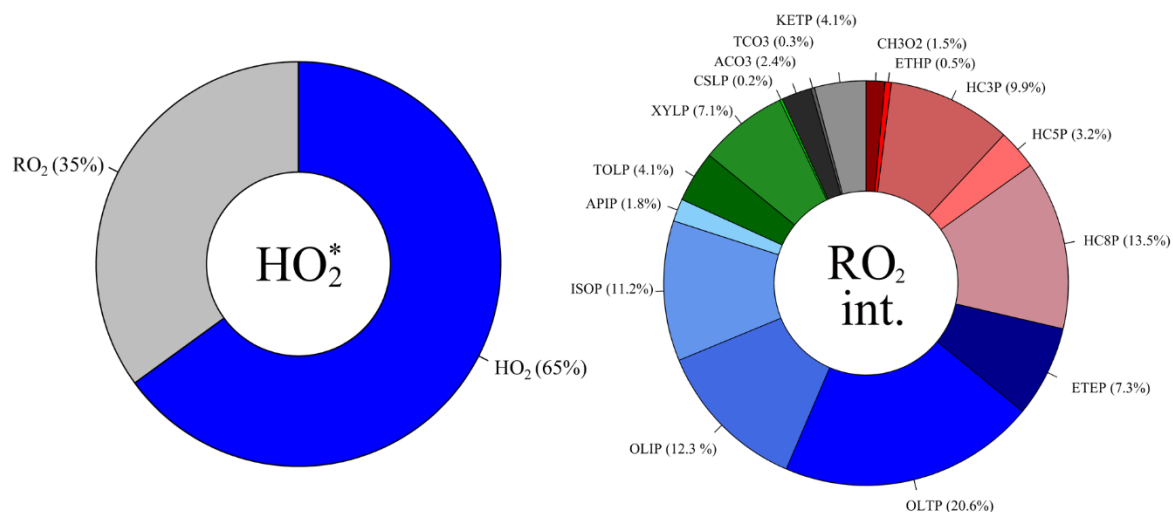


Figure 6. Modeled speciation of the RO₂ interference for MCMA 2006. The pie chart on the left is the modeled HO₂* composition after adding the fraction of RO₂ interference to the modeled HO₂. The pie chart on the right is the composition of the RO₂ interference.

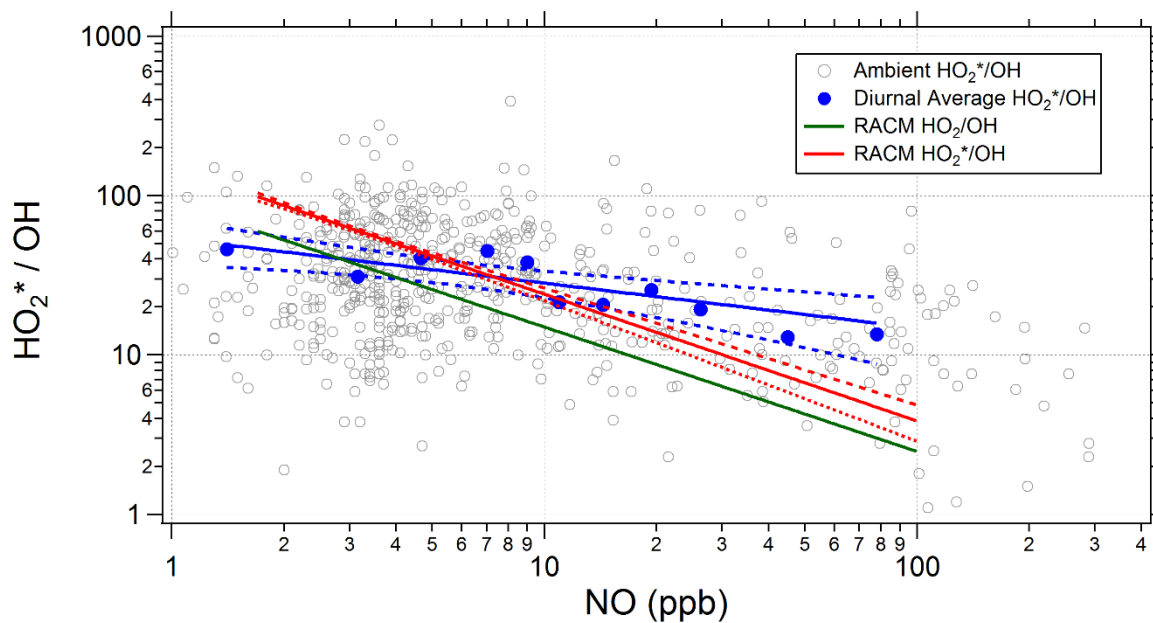


Figure 7. Correlation plot for HO_2^*/OH vs. NO. Small grey circles are individual measurements recorded for the whole campaign. Large blue circles are average values calculated on binned NO data and the blue line is a fit to the average measurements. The model-calculated HO_2/OH ratio is displayed by the green line for the campaign averaged measurements, while the red line represents the modeled HO_2^*/OH ratio. Dashed lines are the 95% confidence interval from the non-linear power regressions.